VCSELs for Atomic Clock Demonstrators

Ahmed Al-Samaneh

We illustrate the output characteristics of two types of 895 nm vertical-cavity surface-emitting lasers (VCSELs) for use in miniaturized Cs-based atomic clocks and report on measurements that indicate the successful operation of clock demonstrators.

1. Introduction

Miniaturized atomic clocks (MACs) [1] are key elements for many applications such as communication systems, remote sensing, and global positioning. Such clocks use the principle of all-optical coherent population trapping (CPT) excitation which does not require a microwave cavity and VCSELs are the ideal light sources. They must feature strictly polarization-stable single-mode emission, have a narrow linewidth at a center wavelength of about 894.59 nm, and be suited for efficient harmonic current modulation at about 4.6 GHz in order to employ the CPT effect at the cesium D1 line [2, 3].

In this article we report some results obtained within the joint European MAC-TFC project [4]. Two different top-emitting oxide-confined VCSEL designs based on the AlGaAs–GaAs material system and InGaAs quantum wells have been utilized, as described in the next two sections.

2. Standard VCSELs

So-called standard VCSELs with a GaAs-substrate-side n-contact and a top annular p-contact (with an associated bondpad) have a circular light output aperture and are not polarization-stabilized. Several such VCSELs have been mounted in TO-46 cans for convenient testing and handling by project partners. The laser chips were fixed on silicon submounts by conductive glue. The anode of the TO can is wire-bonded to the top p-bondpad while the cathode is wire-bonded to the Au-metallized top surface of the Si submount. An external lens is employed for laser beam collimation. A thermoelectric cooler (TEC) and a thermistor are fixed in proximity of the VCSEL package for temperature control. Having no surface gratings, the polarization of the light emitted from standard VCSELs is a priori undefined. Devices with stable polarization in the operation range of interest have been selected. The polarization-resolved light–current–voltage (PR-LIV) characteristics of such a laser are shown in Fig. 1 (left). The threshold currents is around 0.3 mA and has a weak dependence on temperature, namely less than 2 µA/K in a range of 15 to 25°C (not illustrated here). Single-mode emission polarized parallel to the [011] GaAs reference crystal axis is maintained up to a current of 4.4 mA. Over this

range, the orthogonal polarization suppression ratio (OPSR) is greater than 20 dB. It is calculated according to

$$\mathrm{OPSR} = 10 \cdot \log\left(\frac{P_{\mathrm{par}}}{P_{\mathrm{orth}}}\right) \mathrm{dB}\ , \tag{1}$$

where P_{par} and P_{orth} are the optical powers measured behind a Glan–Thompson polarizer whose transmission direction is oriented parallel and orthogonal to the [011] crystal axis, respectively.

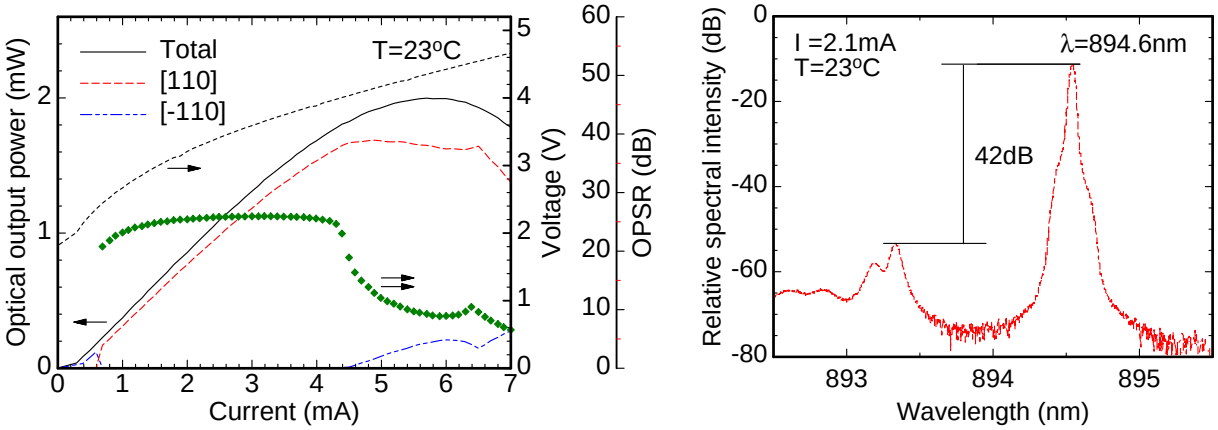

Fig. 1: Polarization-resolved operation characteristics of a standard VCSEL with $D_{\mathrm{a}} = 3\,\mu\mathrm{m}$ at $T = 23°\mathrm{C}$ (left) and its spectrum at $I = 2.1\,\mathrm{mA}$ (right).

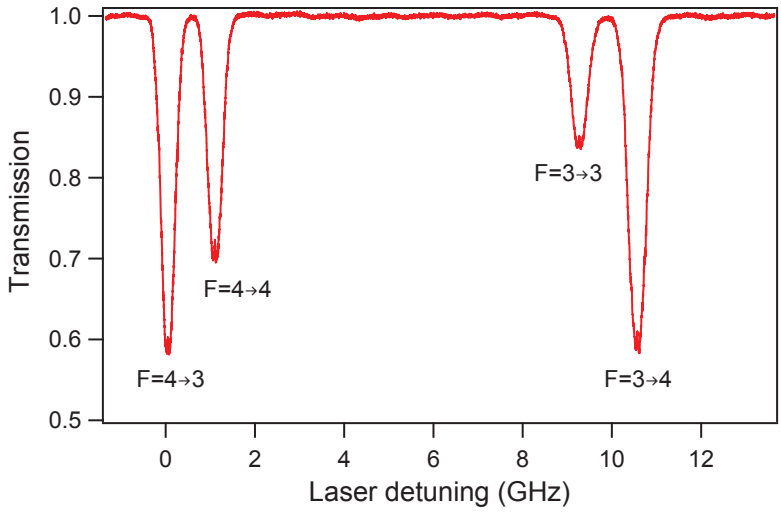

Fig. 2: Cs D_1 absorption lines observed when transmitting the light of the VCSEL from Fig. 1 through a Cs vapor cell (from [5]).

Figure 1 (right) depicts the optical spectrum at 23°C. The Cs D_1 line wavelength of 894.6 nm is reached at a current of 2.1 mA. The output power is 910 µW and the side-mode suppression ratio (SMSR) is about 42 dB. This laser was utilized to resolve all four hyperfine components of the Cs D_1 line, which are clearly separated in Fig. 2. Cs atomic

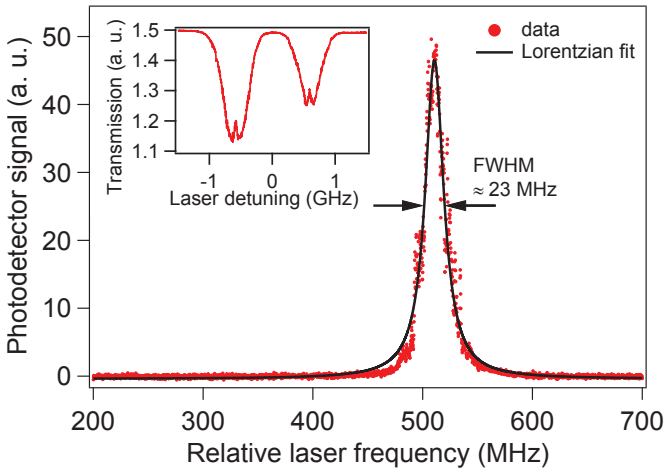

Fig. 3: Emission linewidth spectrum of the VCSEL from Fig. 1 operating at the Cs D_1 line. The Fabry–Pérot linewidth is 5 MHz and the total sweep time for this graph is 30 ms. The inset shows narrow saturated absorption features for the hyperfine transitions $|F = 4\rangle \rightarrow |F' = 3\rangle$ and $|F = 4\rangle \rightarrow |F' = 4\rangle$ of the Cs D_1 line, which were recorded for an evacuated Cs vapor cell (from [5]).

transitions are indicated using the quantum number F associated with the total atomic angular momentum **F**. The laser frequency is detuned over a 14 GHz span at a rate of $\approx$ 300 MHz/µA by sweeping the laser current. The VCSEL was operated at the bias current and temperature from Fig. 1 (right). The Cs absorption maxima appearing at detuning frequencies of 0, 1.2, 9.2, and 10.4 GHz correspond to the $|F = 4\rangle \rightarrow |F' = 3\rangle$, $|F = 4\rangle \rightarrow |F' = 4\rangle$, $|F = 3\rangle \rightarrow |F' = 3\rangle$, and $|F = 3\rangle \rightarrow |F' = 4\rangle$ atomic transitions, respectively, as indicated in Fig. 2. F is designated for the hyperfine structure of the $6^2S_{1/2}$ ground level and F' is assigned to the hyperfine structure of the $6^2P_{1/2}$ excited level. Not well-resolved saturated absorption features can be seen in the four lines. The resolution is improved below in Fig. 3.

2.1 Emission linewidth and modulation sidebands

Figure 3 shows an emission linewidth spectrum of the VCSEL from Fig. 1. The spectrum is measured using a scanning Fabry–Pérot interferometer with 5 MHz intrinsic linewidth and 1 GHz free spectral range. Typical measured full-width-at-half-maximum (FWHM) linewidths are around 20–25 MHz, by which narrow saturated absorption lines can be resolved, as depicted in the inset of Fig. 3. Similar saturated absorption features were reported for the Cs D_2 line at 852 nm wavelength [6]. Such details show that the emission linewidth of the VCSEL is narrower than the linewidths of the Cs absorption lines. Therefore, VCSELs are suitable laser sources for CPT-based atomic clocks in spite of their relatively large linewidths compared to other semiconductor lasers with distributed feedback (DFB) resonator or with an external cavity.

For atomic clock operation, the bias current of the VCSEL from Fig. 1 is modulated by a harmonic signal with a frequency of 4.596 GHz, equal to half the Cs hyperfine ground

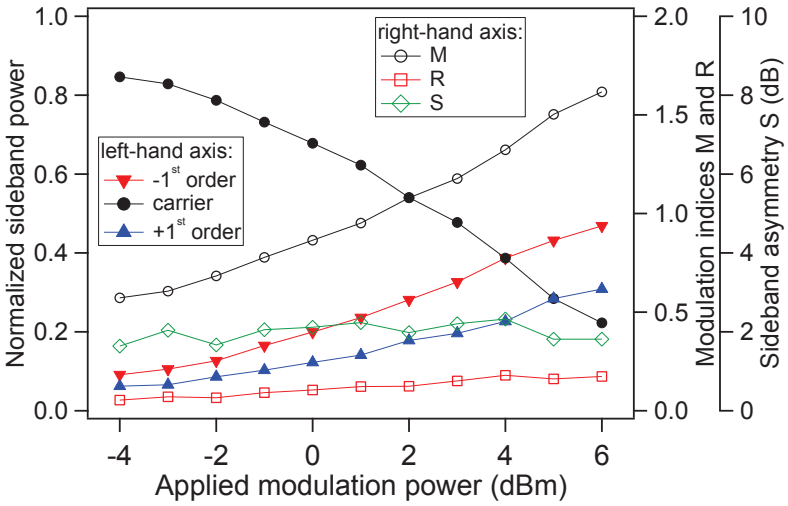

Fig. 4: Normalized power of the carrier and the first-order sidebands (filled symbols, left-hand axis) and corresponding modulation indices M and R and sideband asymmetry factor S (open symbols, right-hand axis) versus the modulation power with, where the 4.596 GHz signal is applied to the VCSEL from Fig. 1 (from [5]).

splitting frequency. This creates modulation sidebands separated by 9.192 GHz, as required for the CPT interaction to take place. Figure 4 shows the relative strengths of the carrier and the first-order sidebands in dependence of the modulation power, measured using a scanning Fabry–Pérot interferometer.

Neglecting any noise contributions, the time-dependent electric field $E(t)$ of light emission from a harmonically intensity-modulated VCSEL can be expressed as

$$E(t) = E_0 \cdot (1 + R\sin(2\pi f t + \phi)) \cdot \cos(2\pi\nu t + M\sin(2\pi f t)) \ , \tag{2}$$

where E_0 is a constant amplitude, ν is the optical carrier frequency, f is the modulation frequency, $R > 0$ and $M > 0$ are the amplitude and phase modulation indices, respectively, and ϕ is the relative phase between both modulations [7]. The modulation indices M and R extracted by fitting the sideband intensities resulting from (2) to the experimental data are depicted in Fig. 4. Also plotted is the asymmetry factor $S = 10 \cdot \log(I_{-1}/I_{+1})$ dB that is the ratio between the intensities in the -1 (lower frequency) and $+1$ (higher frequency) sidebands. As can be seen, $S \approx 2$ dB remains almost constant with applied modulation power, while R slightly changes from 0.05 to nearly 0.18. Both first-order sidebands become stronger than the carrier at modulation powers of $\geq +5$ dBm, and M increases but does not exceed 1.65. According to [8] $\alpha_{\mathrm{H}} = -M/R$, the Henry factor α_{H} increases from -11 to -8.5 over the applied range of modulation powers. The magnitude of α_{H} determined by this method is higher than usually expected. The optimum value of M for the CPT interaction is 1.8, at which most of the modulation modulation power is transferred to the first-order sidebands [9]. Limitations in modulation efficiency can be attributed to imperfect coupling of the modulation signal caused by impedance mismatch between the high-frequency source and the TO-46 can, which was evidenced by approximately 40 % power reflection [5]. Nevertheless, a CPT signal with a narrow linewidth is obtained, as will be shown in Fig. 8.

3. Inverted Grating Relief VCSELs

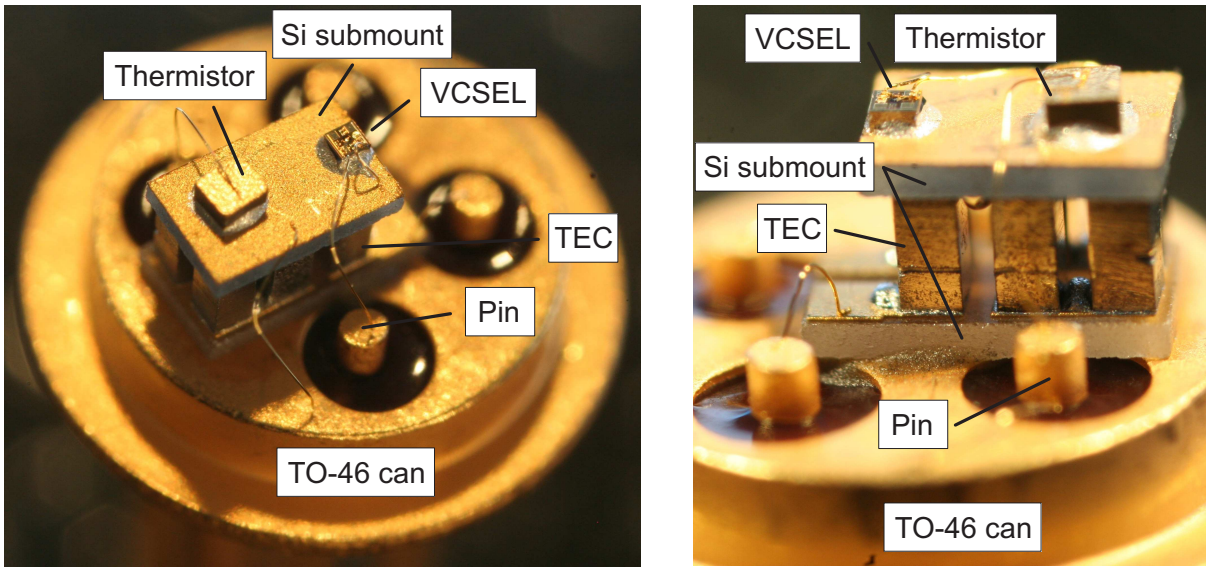

Fig. 5: VCSEL mounted along with a thermistor and a TEC in a TO-46 can (left). Close-up of the assembly taken at a different angle (right). The can has five pins: one for the thermistor, one for the p-pad of the VCSEL, two for operation of the TEC and one as a common ground for all elements. The ground pin is hidden below the lower Si submount.

The second type of VCSELs employed for the clock demonstrators has a flip-chip bondable layout with a top n-contact. In addition, it incorporates an inverted grating relief (IGR) etched into an extra topmost GaAs quarter-wave anti-phase layer of the output facet. In this way, favorable single-mode and polarization-stable laser emission is achieved [2]. Several such lasers have been mounted in TO-46 cans. Having top n-contacts, they were glued on silicon submounts. The anode and cathode of the TO-46 can were wire-bonded to the top p-type and n-type bondpads of the VCSEL. For temperature control, a TEC and a thermistor are placed inside the can, as displayed in Fig. 5.

PR-LIV characteristics of an IGR VCSEL at $T = 30°C$ are shown in Fig. 6 (left). Five times P_{par} is plotted here for better clarity. The device remains polarization-stable up to thermal roll-over with a maximum magnitude of the OPSR of 22.7 dB. The polarization of inverted grating VCSELs with optimum design is always orthogonal to the grating lines, resulting in an opposite sign of the OPSR in Fig. 6 (left) compared to Fig. 1 (left). Figure 6 (right) depicts polarization-resolved spectra at 30°C. The target wavelength is reached at a current of 1.4 mA with SMSR $\approx$ 40 dB and a peak-to-peak difference between the dominant and the suppressed polarization modes of almost 29 dB.

3.1 CPT resonance signal measurements

Figure 7 shows a simplified schematic of an experimental atomic clock setup. For the experiments in this section, the grating relief VCSEL from Fig. 6 in the mount from Fig. 5 is used. It is operated at 1.4 mA and 30°C to reach the Cs D_1 line wavelength, as can be

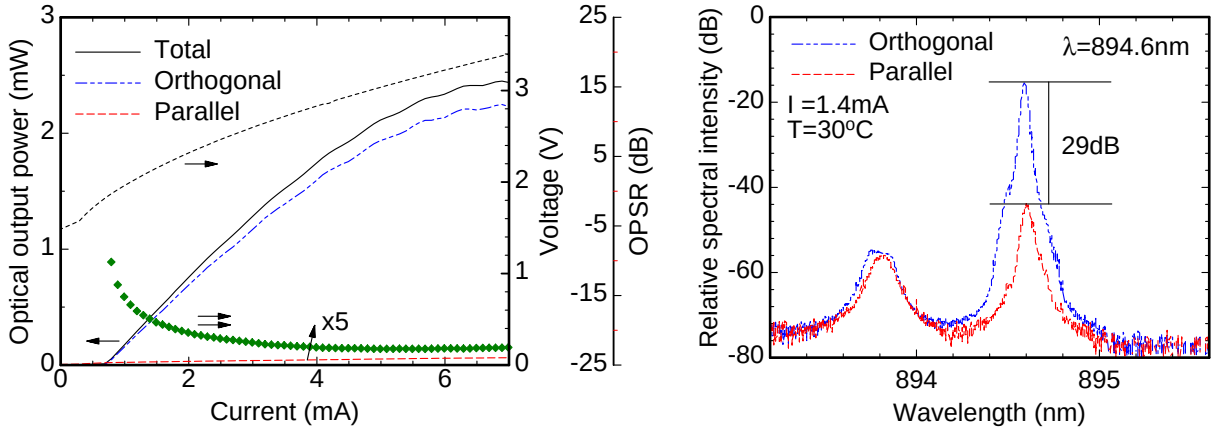

Fig. 6: Polarization-resolved operation characteristics of an IGR VCSEL with 3.6 µm active diameter at $T = 30°C$ (left) and its polarization-resolved spectra at $I = 1.4\,\text{mA}$ (right). The grating relief has a diameter of 3 µm, a grating period of 0.6 µm and an etch depth of 70 nm.

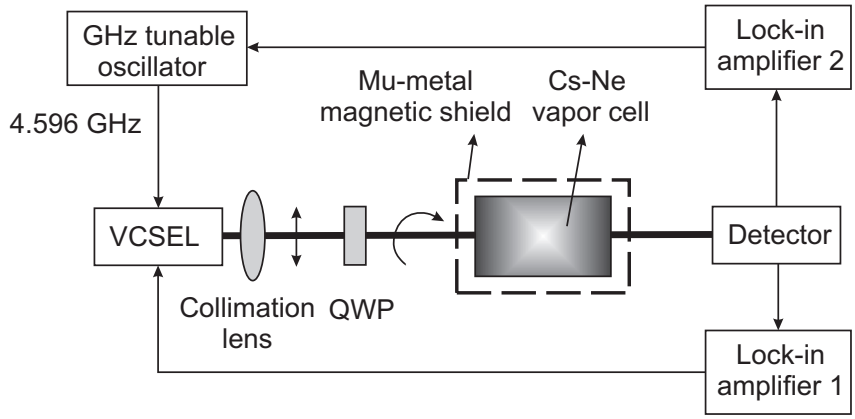

Fig. 7: Simplified schematic drawing of an experimental atomic clock demonstrator.

seen in Fig. 6 (right). The linewidth of the IGR VCSEL is measured to be approximately 25 MHz, which is close to the value of the standard VCSELs.

The optical output of the laser is collimated to a 2 mm diameter beam. The collimated laser beam is then circularly polarized using a quarter-wave plate (QWP) and transmitted through a microfabricated vapor cell. The laser power incident to the cell is about 22 µW. The injection current of the laser is modulated at 4.596 GHz using a commercial frequency synthesizer to produce two modulation sidebands separated by 9.192 GHz, as required for the CPT interaction. The modulation power is set to −2 dBm for a maximum amplitude of the CPT signal. The Cs cell is filled with Ne buffer gas for high short- and long-term frequency stability of the clock. The cell is stabilized to a temperature of ≈ 80°C, at which the sensitivity of the clock frequency to temperature variations is canceled [10, 11]. A static magnetic field of a few µT parallel to the laser beam is applied to split the Zeeman sublevels and enable a so-called σ^+–σ^+ CPT clock scheme on the Cs D_1 line. To prevent the influence of earth or environmental magnetic field perturbations, the cell is placed in a single-layer mu-metal magnetic shield. The σ^+–σ^+ CPT scheme line employs

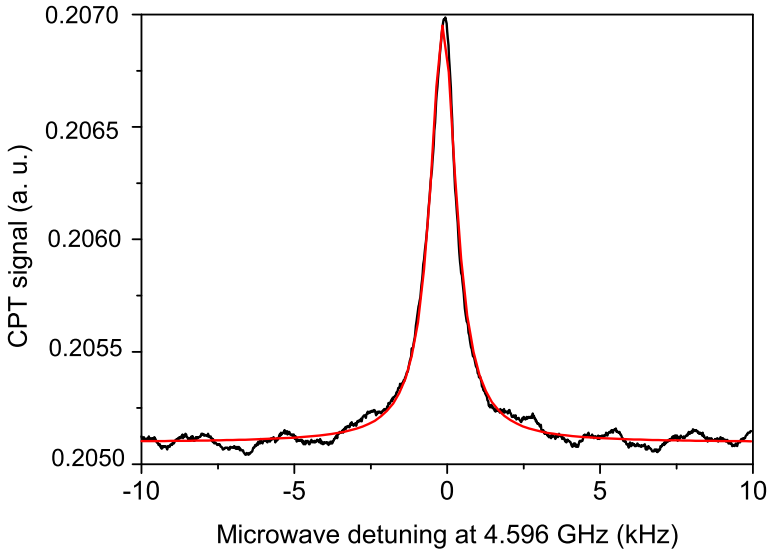

Fig. 8: Measured CPT resonance signal (black line) of a Cs–Ne microfabricated cell along with a Lorentzian curve fit (red line). The temperature of the cell is 80°C (after [5]).

$|F = 3, m_F = 0\rangle$ and $|F = 4, m_F = 0\rangle$ Zeeman sublevels as the two ground energy levels in the Λ-system. The σ^+ optical transition requires circularly polarized light, hence the necessity of the QWP.

The transmitted laser power is detected with a photodiode that provides signals for two lock-in amplifiers. The first one serves to stabilize the laser emission frequency at the Cs D_1 line, while the second provides the CPT signal, which is used to stabilize the GHz tunable oscillator at half of the Cs hyperfine ground splitting frequency. Figure 8 displays a CPT resonance signal obtained at the output of the second lock-in amplifier. The CPT signal is fit by a Lorentzian function. It has a linewidth of 1.04 kHz FWHM and a contrast of 0.93 % (ratio between signal amplitude and background) at 80°C cell temperature [5]. The linewidth does not vary significantly in the 70–90°C temperature range. The expected short-term instability of the clock from the CPT signal is $\sigma(\tau) = 2.9 \times 10^{-11}(\tau/\mathrm{s})^{-0.5}$ at $\tau \approx 1\,\mathrm{s}$ averaging times. The result proves that the developed VCSELs are very good candidates for the realization of high-performance Cs-based MACs [5].

Acknowledgment

We thank D. Setz for help with the processing of an early VCSEL generation and Philips U-L-M Photonics in Ulm for performing most of the VCSEL mounting steps. We acknowledge our MAC-TFC project partners at the Time and Frequency Laboratory (LTF), Physics Department, University of Neuchâtel, Neuchâtel, Switzerland for the characterization of the standard VCSELs (Figs. 2–4) and at FEMTO-ST, CNRS, Besançon, France for the CPT experiments (Fig. 8).

References

[1] S. Knappe, V. Shah, P.D.D. Schwindt, L. Hollberg, J. Kitching, L.A. Liew, and J. Moreland, "A microfabricated atomic clock", *Appl. Phys. Lett.*, vol. 85, pp. 1460–1462, 2004.

[2] A. Al-Samaneh, M. Bou Sanayeh, M.J. Miah, W. Schwarz, D. Wahl, A. Kern, and R. Michalzik, "Polarization-stable vertical-cavity surface-emitting lasers with inverted grating relief for use in microscale atomic clocks", *Appl. Phys. Lett.*, vol. 101, pp. 171104-1–4, 2012.

[3] M.J. Miah, A. Al-Samaneh, A. Kern, D. Wahl, P. Debernardi, and R. Michalzik, "Fabrication and characterization of low-threshold polarization-stable VCSELs for Cs-based miniaturized atomic clocks", *IEEE J. Select. Topics Quantum Electron.*, vol. 19, 1701410, 10 pages, 2013 (error in the caption of Fig. 6: 20°C must be 80°C).

[4] Web page: http://www.mac-tfc.eu; last visited Mar. 2014.

[5] F. Gruet, A. Al-Samaneh, E. Kroemer, L. Bimboes, D. Miletic, C. Affolderbach, D. Wahl, R. Boudot, G. Mileti, and R. Michalzik, "Metrological characterization of custom-designed 894.6 nm VCSELs for miniature atomic clocks", *Opt. Express*, vol. 21, pp. 5781–5792, 2013.

[6] C. Affolderbach, A. Nagel, S. Knappe, C. Jung, D. Wiedenmann, and R. Wynands, "Nonlinear spectroscopy with a vertical-cavity surface-emitting laser", *Appl. Phys. B*, vol. 70, pp. 407–413, 2000.

[7] R. Wynands and A. Nagel, "Inversion of frequency-modulation spectroscopy line shapes", *J. Opt. Soc. Am. B*, vol. 16, pp. 1617–1622, 1999.

[8] C. Harder, K. Vahala, and A. Yariv, "Measurement of the linewidth enhancement factor α of semiconductor lasers", *Appl. Phys. Lett.*, vol. 42, pp. 328–330, 1983.

[9] S. Kobayashi, Y. Yamamoto, M. Ito, and T. Kimura, "Direct frequency modulation in AlGaAs semiconductor lasers", *IEEE J. Quantum Electron.*, vol. 30, pp. 428–441, 1982.

[10] D. Miletic, P. Dziuban, R. Boudot, M. Hasegawa, R.K. Chutani, G. Mileti, V. Giordano, and C. Gorecki, "Quadratic dependence on temperature of Cs 0–0 hyperfine resonance frequency in single Ne buffer gas microfabricated vapour cell", *Electron. Lett.*, vol. 46, pp. 1069–1071, 2010.

[11] R. Boudot, P. Dziuban, M. Hasegawa, R.K. Chutani, S. Galliou, V. Giordano, and C. Gorecki, "Coherent population trapping resonances in Cs–Ne vapor microcells for miniature clocks applications", *J. Appl. Phys.*, vol. 109, pp. 014912-1–11, 2011.